

A Vibrational Technique for *In Vitro* Intraoperative Prosthesis Fixation Monitoring

Seyed Abdolmajid Yousefsani ^{id}, Hooman Dejnabadi ^{id}, Olivier Guyen, and Kamiar Aminian ^{id}, *Senior Member, IEEE*

Abstract—Objective: In this paper, a new vibrational modal analysis technique was developed for intraoperative cementless prosthesis fixation evaluation upon hammering. **Methods:** An artificial bone (Sawbones)-prosthesis system was excited by sweeping of a sine signal over a wide frequency range. The exponential sine sweep technique was implemented to the response signal in order to determine the linear impulse response. Recursive Fourier transform enhancement (RFTE) technique was applied to the linear impulse response signal in order to enhance the frequency spectrum with sharp and distinguishable peak values indicating distinct high natural frequencies of the system (ranging from 15 kHz to 90 kHz). The experiment was repeated with 5 Sawbones-prosthesis samples. Upon successive hammering during the prosthesis insertion, variation of each natural frequency was traced. **Results:** Compared to classical Fast Fourier Transform, RFTE provided a better tracing and enhancement of frequency components during insertion. Three different types of frequency evolving trends (monotonically increasing, insensitive, and plateau-like) were observed for all samples, as confirmed by a new finite element simulation of the prosthesis dynamic insertion. Two main mechanical phenomena (i.e., geometrical compaction and compressive stress) were shown to govern these trends in opposite ways. Follow-up of the plateau-like trend upon hammering showed that the frequency shift is a good indicator of fixation. **Conclusion:** Alongside the individual follow-up of frequency shifts, combinatorial frequency analysis provides new objective information on the mechanical stability of Sawbone-prosthesis fixation. **Significance:** The proposed vibrational technique based on RTFE can provide the surgeon with a new assistive diagnostic technique during the surgery by indicating when the bone-prosthesis fixation is acceptable, and beyond of which further hammering should be done cautiously to avoid bone fracture.

Manuscript received December 20, 2018; revised June 23, 2019 and November 25, 2019; accepted February 3, 2020. Date of publication February 20, 2020; date of current version September 18, 2020. This work was supported by the The Lausanne Orthopedic Research Foundation. (Corresponding author: Kamiar Aminian.)

Seyed Abdolmajid Yousefsani was with the Laboratory of Movement Analysis and Measurement, École Polytechnique Fédérale de Lausanne. He is now with the CamLab at Stanford University.

Hooman Dejnabadi is with the Laboratory of Movement Analysis and Measurement, École Polytechnique Fédérale de Lausanne.

Olivier Guyen is with the Department of Orthopedic Surgery, CHUV-Orthopedic Hospital.

Kamiar Aminian is with the Laboratory of Movement Analysis and Measurement, École Polytechnique Fédérale de Lausanne 1015, Lausanne, Switzerland (e-mail: kamiar.aminian@epfl.ch).

Digital Object Identifier 10.1109/TBME.2020.2974380

Index Terms—Biomedical diagnostics, Combinatorial frequency analysis, Intraoperative prosthesis fixation monitoring, Joint replacement, Vibrational modal analysis.

I. INTRODUCTION

PRIMARY total hip arthroplasty (THA) is one of the most prevalent orthopedic operations with a growing demand due to aging population in developed countries. Based on the 2017 annual report of the American Joint Replacement Registry (AJRR), more than 277,000 primary hip replacement surgeries have been registered from 2012 to 2016 in the United States [1], and estimations reveal that, by the beginning of the coming decade, more than 0.5 million primary THA operations will be conducted per year [2].

Modes of fixation of THA can be cemented, cementless, or hybrid (i.e., one of the acetabular and femoral components cemented and the other one cementless). For cemented implants, a bone cement mantle at the interface between the implant and the bone provides a strong fixation mainly by flowing into the trabecular cavities [3]. Contrarily, cementless fixation is primarily achieved by the intraoperative press-fitting of a surface-coated implant [4] relying on the residual stresses in direct contact with the bone [5]. In longer-term, the cementless implant stability arises from the gradual bone ingrowth to the implant porous coating due to activation of the osteoblastic ossification (i.e., the osseointegration) [6]. The long-term mechanical stability strongly depends on the level of relative movements at the bone-prosthesis interface (i.e., the micromotion) achieved by the initial press fit, although the prosthesis design and surface characteristics and the materials composition are influencing as well [7].

Insufficient press-fitting increases micromotion under physiological loading. An excessive micromotion beyond a critical threshold (between 50 and 150 μm) activates a fibrous tissue formation rather than the osseointegration [8] and stimulates an osteoclastic bone resorption response. This may result in failure secondary to aseptic loosening [6], [9], with potential prosthesis migration [10].

On the other hand, excessive press-fit of the stem in cementless THA does not provide any advantage in terms of initial fixation, but increases the risk of intraoperative periprosthetic fractures [11] due to excessive hoop stress [5], particularly (but not only) in osteoporotic and elderly patients, with an incidence rate of 3–18% of primary THAs and up to 17.6% [12] and 30%

[13] of THA revision cases. This clearly indicates how crucial and technically demanding the initial press-fit fixation is in order to achieve adequate stability.

To achieve an optimum bone-prosthesis fixation intraoperatively orthopedic surgeons mainly rely on their own experience [11] by noticing the change of sound heard upon the successive hammer impactions [5]. Digital radiography assisted THA provides an intraoperative diagnostic technique to assess the prosthesis seating during the surgery; however, it is more helpful to assess the position and orientation of the implants than to assess the quality of the fixation. In addition, because of radiation, its use remains limited in practice [14].

In recent years, non-imaging techniques in the framework of vibrational analysis of the bone-prosthesis system (also known as vibrometry, modal analysis, etc.) have been developed for intraoperative fixation evaluation [5], [7], [11], [15]–[19], osseointegration assessment [20]–[23], and postoperative loosening diagnosis [24]–[32]. Development of instrumented (sensor-integrated) prostheses [22], [27], [28], [33], [34] with telemetric systems for in vivo monitoring [35], [36], establishment of new techniques based on acoustics [23], [34], use of ultrasound probes instead of conventional sensors like accelerometers [30], and extracorporeal shockwave excitation [31] are amongst the recent efforts towards the vibrational analysis of the bone-prosthesis systems.

Vibrational analysis is an inexpensive, simply performable, non-invasive technique that works based on discrimination between the vibrational characteristics (including the frequency spectrum or the frequency response function and the natural frequencies) of a poorly-fixed (or loose) bone-prosthesis system and a well-fixed (or secure) one. In comparison with radiography, vibrational analysis has shown 20% more sensitivity in discrimination of loosening [25]. Actually, a secure bone-prosthesis system, when subjected to a vibrational excitation, behaves linearly as a unified system with no harmonics or distortions in the frequency spectrum, whereas a poorly-fixed or severely loose prosthesis is characterized by the appearance of harmonics and wave distortions in the frequency spectrum or by the natural frequency shifts to lower values as a result of the system stiffness reduction [18].

A system at the early stages of loosening, however, behaves almost linearly [25]. This is also the case at the intermediate stages of prosthesis insertion during the surgery, when the stem is well seated, but the final fixation is still not achieved. In these challenging cases, higher vibrational modes should be excited, considering that higher natural frequencies are more sensitive to the prosthesis stability [36], [37], and vibrational analysis at low frequencies is capable of detection of only severely loose prostheses [26].

In most of previous studies the bone-prosthesis system was excited over a narrow frequency band (e.g., <1 kHz [25], [26], 0.1–1.2 kHz [24], 0.1–1.5 kHz [30], 1.2–2 kHz [17], [19], 0.1–2 kHz [29], and 0.03–3 kHz [32]). However, the most sensitive band for excitation was found above 4 kHz during the insertion of prosthesis in a THA [11], and between 12 and 15 kHz for the shoulder joint [18]. Consequently, the bone-prosthesis system should be excited up to high frequencies in order of

tens of thousands of Hertz, considering that compared to narrow and low frequency, higher modes are more sensitive to lack of geometrical integrity. But the excitation of higher modes and extraction of associated natural frequencies by processing the frequency response function are great challenges for this end.

Use of the impulse method [5], [15], [16], [18], [20] to excite higher modes is somehow challenging because of high structural damping. In the impulse method, the output signal of the system in response to an impulsive force is exactly its impulse response signal, which is very short in duration and has a low signal-to-noise ratio due to the limited power supplied to the system. Therefore, the impulse response signal obtained by this method is not rich enough for the extraction of natural frequencies of particularly higher modes. Besides, exertion of a single-hit impulsive force with a fully elastic contact and the sensor saturation prevention are challenging as well.

Contrarily, when the system is excited either by stepped or continuous sine sweep over a wide frequency band [6], [9], [21], [23], [30], [33], [34], [36] there would be enough time and energy for excitation of even higher modes, and all the resonances in the swept band are passed [38]. Hence, the signal-to-noise ratio is considerably higher compared to the impulse method, and a clear distinction of the linear impulse response signal from nonlinear distortions is also possible. Despite many advantages, a stepped sine sweep takes long time in case of sweeping up to high frequencies. This time could be reduced by a continuous exponential sine sweep (ESS) with varying frequency over a short-time duration [39].

In this paper, a new vibrational analysis technique is developed for the intraoperative prosthesis fixation evaluation using artificial bone-prosthesis model. The new technique is based on ESS for exciting the prosthesis over a wide frequency range and a new mathematical technique to determine the linear impulse response of the system by prolonging the impulse response and enhancing higher natural frequencies with almost sharp peaks. Then upon successive hammer impactions the evolution of natural frequencies of the system is evaluated and a new safety criterion for the hammer impaction progress is suggested based on combinatorial analyses of different frequency evolution trends. The results are compared to conventional FFT and to numerical finite element model of the system.

II. METHODS

First, the proposed vibrational measurement technique is introduced. Then the specifications of experimental setup and measurement protocol are described in details. Finally, a new finite element model of the system is developed to simulate the underlying dynamic phenomena during the stem insertion.

A. Vibrational Measurement Technique

A two-step procedure is defined here to obtain the frequency spectrum of the system and the associated vibrational characteristics using the excitation (input) and the response (output) signals of the system. In the first step, the ESS algorithm, developed by Farina [39], is used to determine the system linear impulse response (simply named $h(t)$ hereafter). Then,

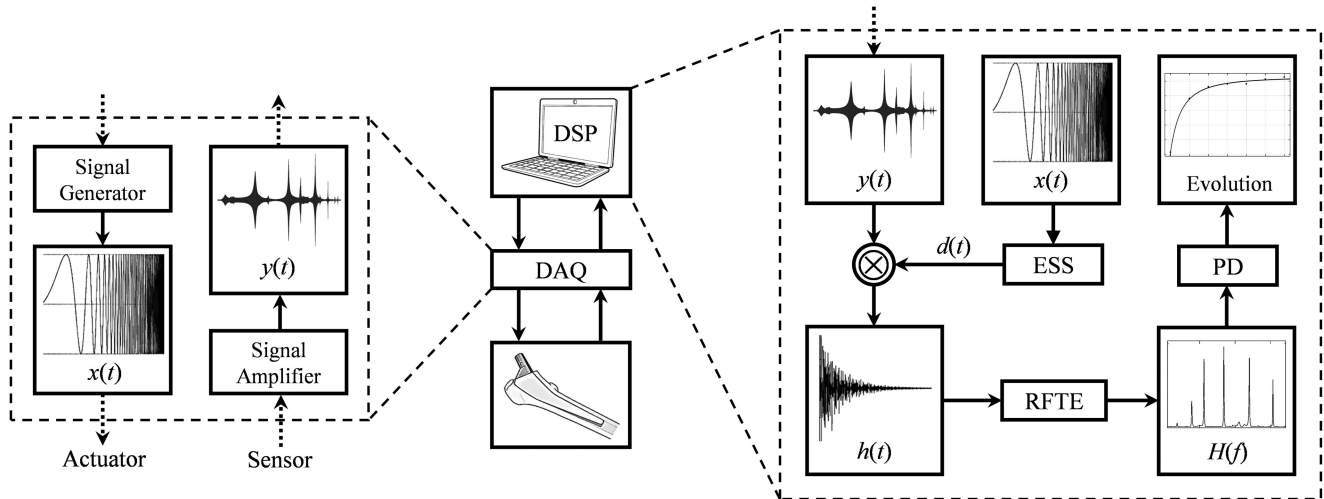


Fig. 1. Schematic view of the vibrational measurement technique. The excitation signal $x(t)$ and response signal $y(t)$ are analyzed by DSP unit to obtain the linear impulse response signal $h(t)$ and the enhanced frequency response function $H(f)$ for peak detection.

a new mathematical technique based on the signal enrichment, named the “recursive Fourier transform enhancement” or simply RFTE, is applied to the linear impulse response signal to obtain the enhanced frequency response function of the system, $H(f)$, with much more sharp and distinct peaks compared to transfer function obtained through simple FFT. In this way, a peak detection operation (PD) can simply apply a proper threshold to $H(f)$ signal and pick out the associated natural frequencies of the system automatically. Finally, the evolution of different natural frequencies of the system upon consecutive hammering is traced. By introducing an appropriate safety criterion the surgeon can decide when to stop hitting more reliably. Fig. 1 depicts the proposed approach schematically.

The system under investigation is excited by a continuous exponential sine sweep signal (also known as the “logarithmic sweep”) over a wide frequency band from 800 Hz to 96 kHz (half of sampling rate) according to [39]. The swept-sine signal is generally written as:

$$x(t) = \sin \left[\frac{Tf_1}{\ln(f_2/f_1)} \left(e^{\frac{t}{T} \ln(f_2/f_1)} - 1 \right) \right] \quad (1)$$

It takes T seconds to sweep over an angular frequency band starting at f_1 and ending at f_2 . This signal is generated with the exponential variation of the instantaneous frequency between these values. Without loss of generality, for a linear time-invariant system, the output signal, $y(t)$, equals to the input signal, $x(t)$, convolved by the linear impulse response, $h(t)$, as:

$$y(t) = x(t) \otimes h(t) \quad (2)$$

A deconvolution filter function, $d(t)$, is defined so that when convolved by $x(t)$ results in the Dirac delta function. That is,

$$x(t) \otimes d(t) = \delta(t) \quad (3)$$

By convolving both sides of (2) with $d(t)$ and substituting (3) into the resultant, $h(t)$ can be obtained as:

$$h(t) = y(t) \otimes d(t) \quad (4)$$

If the deconvolution filter is known, (4) simply gives the linear impulse response of the system with regards to its response signal. According to (3), the deconvolution filter is obtained as:

$$d(t) = \text{IFFT} (1/\text{FFT} (x(t))) \quad (5)$$

where FFT and IFFT stand for the Fast Fourier Transform and its inverse operators, respectively. The obtained deconvolution filter $d(t)$ is the time-reversal mirror of the input signal [40], which is generated as described in [41].

Next step is to calculate the frequency response function, where generally consisted by the application of FFT to $h(t)$. However, because of high structural damping, $h(t)$ is too short in duration in order of only a few milliseconds. A normal FFT, therefore, is unable to pick out the natural frequencies with sufficient resolution needed for automatic peak detection procedure in the last step. To overcome this challenge, the RFTE (which is also known as the extended discrete Fourier transform [42]) is implemented to enrich the impulse response signal mathematically [42]. The enhanced frequency response function, $H(f)$, then can be obtained as:

$$H(f) = \text{RFTE} (h(t)) \quad (6)$$

The RFTE reproduces a prolonged signal by the virtual extrapolation of the actual signal in the time domain in a recursive manner. Hence, resolution of the frequency spectrum increases [42]. Using the enhanced frequency response function the vibrational characteristics of such a highly-damped bone-prosthesis system can be determined more accurately.

$H(f)$ is then post-processed to determine the dominant natural frequencies. A peak detection algorithm is applied to $H(f)$ signal to distinguish the peak values corresponding to distinct natural frequencies. Firstly an amplitude threshold, which is set to one tenth of the maximum peak value in the frequency spectrum, applies to $H(f)$ to eliminate low amplitude frequencies and unwanted noises. Then a reasonable bound of variation, in order of few hundred Hertz, is defined as a search range in vicinity of each high amplitude peak. This range is defined based on a

TABLE I
SPECIFICATIONS OF THE SELECTED PROSTHESIS AND SAWBONES BLOCKS

	Material	Density	Volume ratio	Elastic Modulus	Size
Sawbones Block	Solid Polyurethane Foam	0.24 g/cm ³	20%	123 MPa	65mm×180mm×40mm
Femoral Prosthesis	Anodized TA6V (Titanium Alloy)	4.43 g/cm ³	-	110000 MPa	Size 4 in catalogue (144.9mm×14.5mm)

preliminary measurement on variations of frequencies within the test. The maximum value within each bound is determined as the associated natural frequency, an algorithm known as labeling. In this way, only the vibration modes which remain strong enough (with high amplitude and sharp peak) and easily distinguishable (with no other modes in their vicinity) during the whole insertion steps will be selected for the follow-up. Moreover, if any new mode appears close to a previously labelled mode, both of them are withdrawn. After each step of hammer impact, the above procedure is performed, and the evolution of modal frequencies are analyzed consecutively.

B. Materials

The proposed vibrational analysis technique for intraoperative fixation monitoring was implemented on a cementless operation conducted on artificial bone samples. To mimic the mechanical properties of the cancellous bone, which is in direct contact with the prosthesis during the insertion, solid rigid polyurethane foam blocks (Sawbones, Vashon, Washington 98070, USA) were used. Manufacturer claims [43] this foam as the most commonly used artificial material for testing the screw pullout, insertion and stripping torque, and although not replicating the actual cancellous bone structure, this artificial material comparably reflects the in-range mechanical properties, which makes it a standard synthetic material for testing of orthopaedic devices and medical instruments. The Integrale femoral stem (Amplitude, 26000 Valence, France) was used as a standard prosthesis for the cementless THA. This is a straight femoral implant with full hydroxyapatite (HAP) coating applicable for the primary hip replacement. Mechanical properties and geometrical details of Sawbones blocks and selected prosthesis are listed in Table I.

C. Experimental Measurement Setup

The measurement system consists of a personal computer equipped with an authorized software for the acoustics and vibration analyses (EddySonix, 1350 Orbe, Switzerland) as the digital signal processing (DSP) unit, a soundcard model Audiointerface UR44 with sampling rate of 192 kHz and resolution of 24-bit (Steinberg, 20097 Hamburg, Deutschland) as the data acquisition (DAQ) unit, a driver/charge amplifier (Lehle GmbH, D-46562 Voerde, Germany), and a set of piezoelectric pickups (DiMarzio and K&K sound pickups) for sending/receiving the signals. To keep the signal strength as high as possible, both the sender and receiver are attached to the prosthesis itself with a face-to-face configuration. We also performed the excitation and measurements in different directions and obtained almost the same results. Moreover, to eliminate the vibrational artefacts that may be introduced during the measurement, the system is

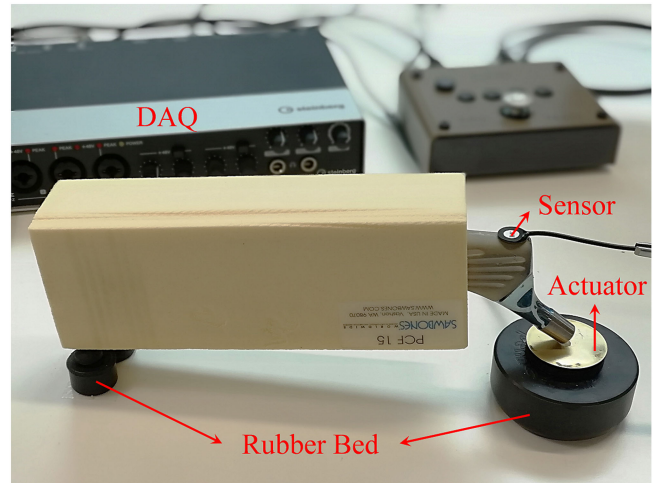


Fig. 2. Experimental measurement setup.

suspended on an acoustically isolated bed consisting of rubber supports. The direct metal-to-metal contact and the associated interfacial low-magnitude oscillations at resonance frequencies is also avoided by attaching both sender and receiver pickups by a thin layer of silicon rubber, which is a perfect guide for wave propagation. Fig. 2 shows the experimental setup.

To prepare the Sawbones blocks for the insertion, they were fixed primarily and drilled with a vertical hole as a guide for reaming. Then reamers were used to enlarge the hole to a conical shape. Appropriate seating cavity was finally achieved stepwise in each sample block by sequential rasping from level 1 to 4. All the preparation steps and insertion processes were accomplished by an experienced orthopaedic surgeon using a full set of surgical instrumentation kit.

Measurement starts with the manual insertion of the femoral stem into the rasped cavity so that a direct contact is achieved between two parts. Baseline vibrational measurement step (S_0) is conducted while the prosthesis-Sawbones system is suspended on the isolated bed. The first hammer impactation is then exerted to the stem, when it is distally fixed, putting effort to hit at a level similar to the real surgical operation. Afterwards, the first vibrational measurement step (S_1) is performed on the system when it is suspended on the isolated bed. The consecutive hammer impact followed by the vibrational measurement steps (S_2, S_3 , etc.) continues likewise until the surgeon decides on the final fixation. It is noticeable that in the above procedure the hammer is hit with a controlled force except for the last two or three impacts to forcefully move the prosthesis down and mimic the critical uncontrolled situation. We assume when

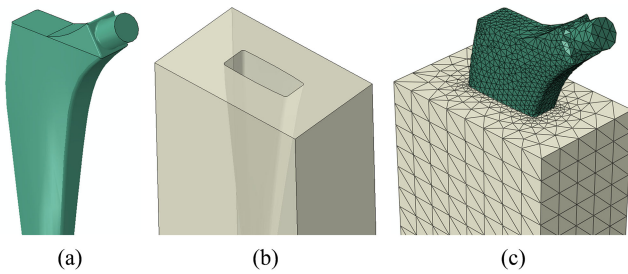


Fig. 3. Geometrical models of (a) prosthesis, (b) rasped Sawbones block (transparent view), and (c) assembly of the meshed instances.

relative insertion displacement decreases to zero, the natural frequencies are no longer changing after a number of impacts unless the last two or three impacts are hit much stronger.

D. Numerical Simulation

To have a better insight of the mechanics of prosthesis insertion, a new finite element model is developed using the commercial finite element software ABAQUS, in which the dynamic insertion of the prosthesis into the Sawbones block is simulated by means of numerical modal analysis. The simulation is aiming to confirm our hypotheses on the mechanical phenomena governing the frequency evolution rather than quantitative comparison between numerical and experimental results. So to avoid intensive mesh size reduction which increases the computational costs three-dimensional geometry of Integrale femoral stem was slightly simplified (i.e., lateral grooves and corner fillets were not modeled) and modeled using the computer aided design software SolidWorks. Unlike its bulk properties, these marginal simplifications do not significantly change the mechanical characteristics of prosthesis.

The Sawbones block component was also modeled as a rectangular cuboid, which is firstly cut-extruded by a vertical hole, and then subtracted by the geometry of the final rasping tool (level 4). In this way, the seating cavity for the stem insertion was achieved. Fig. 3 illustrates geometrical models of the parts as well as the assembly. Both components are modeled as homogeneous solid parts with isotropic elastic properties as listed in Table I (with Poisson ratio of 0.3), and meshed by the standard four-node linear tetrahedron elements (C3D4) with an average edge length of 1 mm. To ensure the independency of results to the mesh size and density, a mesh convergence study is performed and both geometries are meshed with a fine seed at the interfaces as illustrated in Fig. 3.

The interaction between the parts was defined as standard surface-to-surface contact with the finite sliding control, and the prosthesis peripheral surface was selected as the master surface. The normal and tangential interaction properties were modeled by linear contact with stiffness of 1200 N/mm and penalty friction formulation with a coefficient of 0.4, respectively [44]. The insertion procedure was simulated similar to the experimental testing. Each stage of insertion modeling and vibrational analysis includes three steps:

- *Dynamic loading*: the hammer impact is simulated by the exertion of an axial compressive load L , distributed normally on a small surface at the top of the stem model. The force is applied within 10 ms in a dynamic implicit analysis, whereas the block is fixated distally similar to the hammering step in the experimental conditions.
- *Static unloading*: the simulation continues to a no-load static step to recover the steady-state conditions after the removal of the dynamic load and before conducting the modal analysis.
- *Vibrational modal analysis*: natural frequencies of the model are then obtained in a modal frequency analysis with the distal constraints removed.

Numerical simulation procedure described above begins with the application of a dynamic compressive load $L = 0.2$ kN as an approximation of the manual load during the baseline insertion of the prosthesis, and continues to static unloading and the baseline vibrational modal analysis noticed by S_0 . Then for each next stage of insertion (S_1, S_2, \dots) these modeling steps (i.e., dynamic loading, static unloading, and modal analysis) are conducted consecutively considering that the compressive load L increases by 1 kN at each dynamic loading step.

III. RESULTS

A. Experimental Results

The proposed experimental testing and measurement protocol was conducted on 5 identical Sawbones blocks. After each hammer impact, the vibrational measurement technique was repeated 3 times to ensure the repeatability of the measurement. The insertion depth was also measured after each hammer impact. The relative position of a fixed point on the prosthesis was initially measured with respect to a fixed point on Sawbones block (as the reference) at the initial fixation step. After each hammering step difference between the current relative position and the initial value indicates the insertion depth. In what follows, the results are first reported for a typical prosthesis-Sawbones sample, and then repeated for all other samples.

The continuous excitation swept-sine signal in (1) was generated considering that $f_1 = 800$ Hz, $f_2 = 96$ kHz (half of the sampling rate), and $T = 30$ s. Fig. 4(a) shows the time-domain output signal $y(t)$ in gray measured for a typical prosthesis-Sawbones sample at the baseline insertion step (S_0). The corresponding time-domain linear impulse response signal $h(t)$ obtained by the application of ESS technique is shown in blue in Fig. 4(b). Note that $h(t)$ lasts in only few milliseconds because of high structural damping. Then $h(t)$ is virtually extrapolated in time domain by the application of RFTE as shown in red in Fig. 4(b). The frequency spectrums obtained through the application of FFT on signal $y(t)$ (i.e., $\text{FFT}(y)$ shown in gray in Fig. 5(a)) and signal $h(t)$ (i.e., $\text{FFT}(h)$ shown in blue in Fig. 5(b)) are compared to the frequency spectrum obtained by RFTE (i.e., $H(f)$ shown in red in Fig. 5(b)) where the extended linear impulse response signal was used. It is noticeable in Fig. 5 that the $\text{FFT}(y)$ is noisy, while $\text{FFT}(h)$ suffers from low resolution, flat and lower amplitude

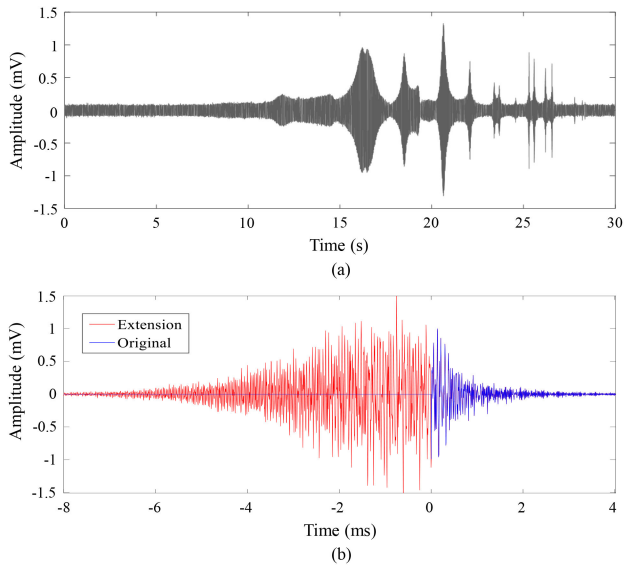


Fig. 4. (a) Response signal $y(t)$ measured for a typical prosthesis-Sawbones sample at the baseline insertion step (S_0) and (b) corresponding original linear impulse response signal $h(t)$ in blue and its extension in red (obtained by RFTE).

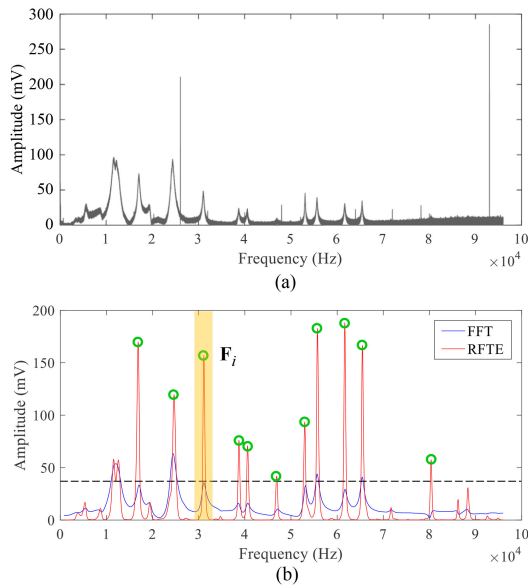


Fig. 5. Comparison between the FFT and RFTE techniques for a typical prosthesis-Sawbones sample at the baseline insertion step (S_0), (a) FFT of measured raw output $y(t)$, $FFT(y)$ and (b) FFT of original linear impulse signal $h(t)$, $FFT(h)$ in blue and the response function $H(f)$ in red obtained by RFTE. The amplitude threshold for peak detection algorithm (PD) is indicated by a horizontal black dashed line, the frequency search range in vicinity of a sample frequency F_i is highlighted in orange. The peak values corresponding to the natural frequencies (green circles) are better detected by RFTE.

peaks compared to $H(f)$ and therefore all peak frequencies cannot be correctly detected after application of threshold.

As illustrated in Fig. 5(b), each peak value F_i in $H(f)$ corresponds to the i th distinguishable and high amplitude peak,

TABLE II
LABELED NATURAL FREQUENCIES OF A TYPICAL PROSTHESIS-SAWBONES SAMPLE AT THE BASELINE INSERTION STEP (S_0)

Label	Frequency (Hz)			Dev. (%)
	Trial 1	Trial 2	Trial 3	
F_1	16994	16994	16994	0.00
F_2	19409	19420	19409	0.06
F_3	30871	30871	30871	0.00
F_4	38606	38618	38606	0.03
F_5	40517	40517	40505	0.03
F_6	53022	53010	53010	0.02
F_7	55577	55577	55577	0.00
F_8	61590	61590	61601	0.02
F_9	65387	65387	65387	0.00
F_{10}	69044	69044	69020	0.03
F_{11}	71610	71610	71610	0.00
F_{12}	80377	80377	80377	0.00
F_{13}	86225	86214	86225	0.01

Normalized deviation, Dev. (%), for each F_i is defined as the ratio of maximum difference between trials to the median.

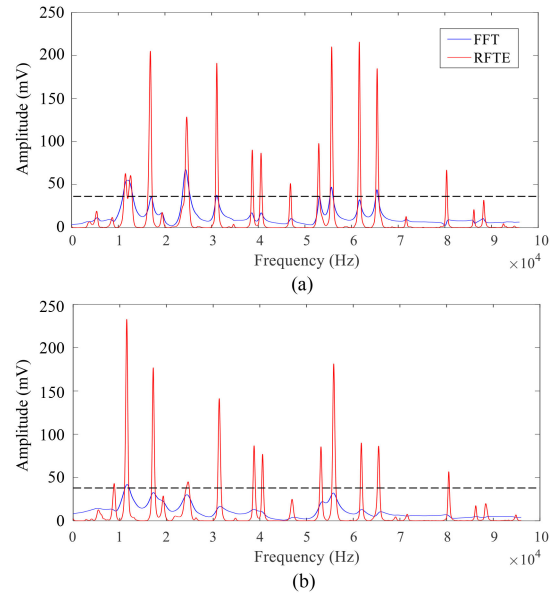


Fig. 6. Comparison of frequency spectrums $FFT(h)$ and $H(f)$ at two different insertion steps (a) S_3 and (b) S_{11} . Dashed line in black shows the peak detection threshold.

which may not necessarily coincide to the actual i th natural frequency of the system. Table II shows three measurement trials for each labeled natural frequency at the insertion step S_0 . The normalized deviation, defined as the ratio of maximum difference between trials to the median, has also been reported for each natural frequency F_i . As it can be seen, negligible deviations confirm the repeatability of the measurements.

The frequency extraction and labeling procedures should be performed after each hammer impact step. Fig. 6 compares the frequency spectrums $FFT(h)$ in blue and $H(f)$ in red at the insertion steps S_3 and S_{11} . Frequency peaks in $FFT(h)$ are wide and weak, suffering from damping which increases by further insertion of prosthesis. However, in $H(f)$ most of vibration modes remain strong enough with still sharp and distinguishable peaks

TABLE III

EVOLUTION OF NATURAL FREQUENCIES OF A TYPICAL PROSTHESIS-SAWBONES SAMPLE UPON SUCCESSIVE HAMMERING COMPARED TO BASELINE (S_0)

D (mm)	Hammering Step													
	S_0 (baseline)	S_1	S_2	S_3	S_4	S_5	S_6	S_7	S_8	S_9	S_{10}	S_{11}	S_{12}	S_{13}
0.0	0.0	0.9	1.8	2.3	2.7	3.1	3.5	3.8	4.0	4.4	4.9	5.0	5.5	6.3
	Natural Frequency (Hz)													
	Baseline	Shift from baseline												
F_1	16994	35	47	82	105	105	117	141	164	164	176	211	234	270
F_2	19409	12	24	24	24	12	24	24	24	12	0	12	12	12
F_3	30871	35	70	117	141	152	164	176	211	188	188	211	234	223
F_4	38606	23	47	70	82	94	106	117	106	106	94	94	82	59
F_5	40517	12	12	23	35	23	23	35	35	12	12	23	0	-24
F_6	53010	12	47	59	82	82	94	94	106	106	94	106	106	94
F_7	55577	23	47	70	82	94	106	106	129	129	129	141	141	141
F_8	61590	24	35	35	24	70	59	59	82	82	59	82	47	59
F_9	65387	12	12	35	35	35	35	47	59	59	59	59	47	47
F_{10}	69044	23	35	29	47	35	35	47	64	35	105	76	29	141
F_{11}	71610	0	23	35	47	59	59	82	82	82	94	94	152	94
F_{12}	80377	0	12	12	12	12	12	12	23	12	12	12	0	-12
F_{13}	86225	-24	-12	0	0	12	12	23	35	47	59	47	70	135

D corresponds to the absolute insertion depth in mm.

during the whole insertion steps. With the data collected in this way, the evolution of all distinct natural frequencies can be easily followed up. Table III shows the median of the three measured natural frequencies at the baseline step (S_0) as the reference state, as well as the frequency shifts with respect to the baseline value and the absolute insertion depths, D , after consecutive hammering steps.

There were many modes appearing in the range of 800 Hz to 96 kHz (>30 frequencies) only one-third of which met the requirements for peak detection and labeling, as reported in Table III. Among the data reported in this table, the plots of frequency are illustrated in Fig. 7. For the purpose of a meaningful comparison, all graphs are plotted in the same scale. As it can be seen, the frequency evolution behavior is categorized into three main groups: Group A (e.g., F_1) with a monotonically increasing behavior reflects an almost uniform increase of the natural frequency in response to a uniform increase of the insertion depth, Group B (e.g., F_{12}) with an insensitive behavior shows almost no significant variation with the insertion progress, and Group C (e.g., F_4 , F_6 , and F_7) with a plateau-like behavior indicates that the associated frequency increases upon the hammer impact until it reaches a plateau and then decreases to some extent. Results of other frequencies can be categorized into these three main groups (i.e., F_8 , F_{10} , F_{11} , and F_{13} in Group A, F_2 and F_5 in Group B, and F_3 and F_9 in Group C).

Within each group of frequencies, intra-group combinatorial analyses were also performed by estimating difference and ratio of frequencies. As an example, Fig. 8 shows the most indicative variations of intra-group frequency differences (i.e., F_7-F_4 and F_6-F_4) and frequency ratios (i.e., F_7/F_4 and F_6/F_4) in Group C. Similarly, the inter-group combination between the frequencies of different groups was performed. Fig. 9 shows the most indicative variations of the inter-group frequency differences (i.e., F_4-F_1 , F_6-F_1 , and F_7-F_1) for groups A and C.

Similar results were found for all prosthesis-Sawbones samples as well. Since the insertion depth after an intended hammer impact may not be identical for all prosthesis-Sawbones

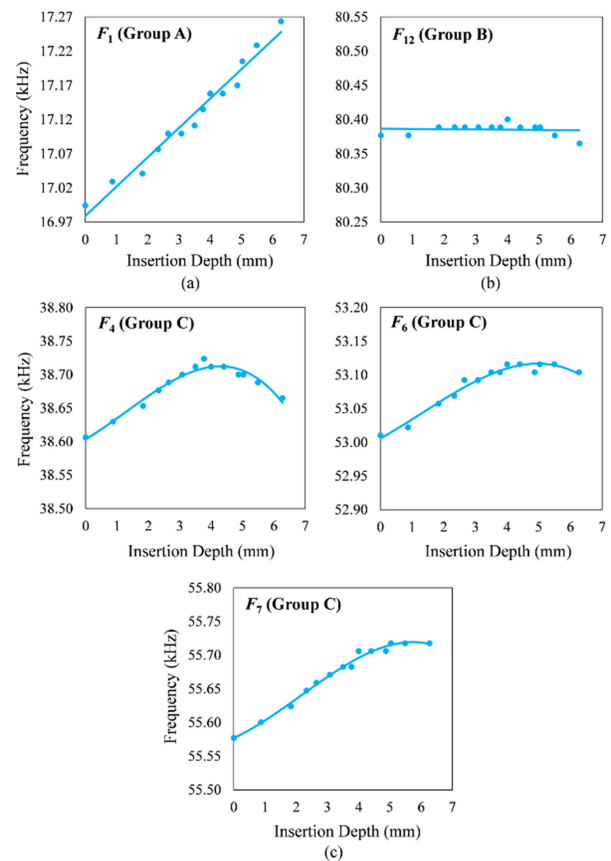


Fig. 7. Frequency evolution upon hammering of five indicative natural frequencies grouped in three distinct categories: (a–c) Groups A, B, and C with respect to insertion depth of a typical prosthesis-Sawbones sample.

samples, a linear interpolation was applied to all data to make them comparable at equal insertion depths. Fig. 10 illustrates the three different behavior indicated by Groups A, B, and C in terms of the mean values (depicted by a solid line) and standard

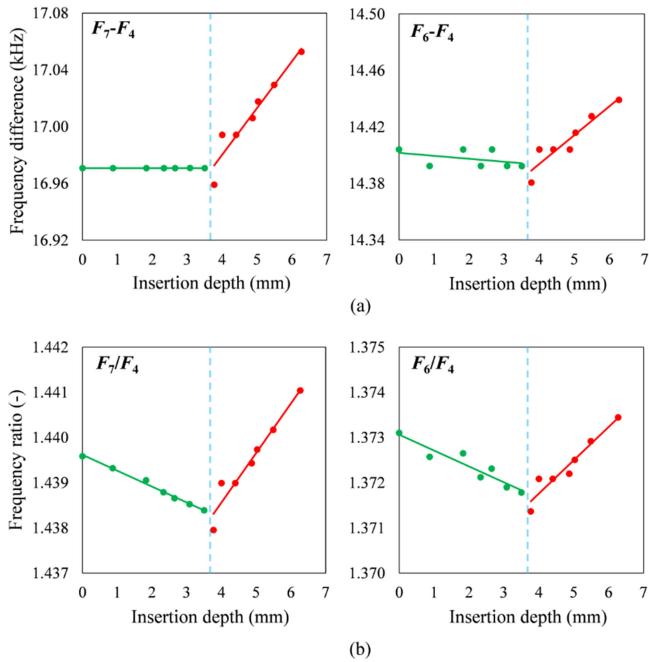


Fig. 8. Variations of intra-group frequency combinations in Group C with respect to insertion depth upon hammering, (a) the frequency differences and (b) the frequency ratios.

deviations (depicted by a shaded region) measured for all the prosthesis-Sawbones samples.

B. Simulation Results

Numerical simulation results indicate that the evolution of natural frequencies of the prosthesis-Sawbones model during the hammer impact simulation can be categorized into the same three groups as the experimental results. The frequency evolution plots of three indicative sample frequencies of each group are depicted in Fig. 11. For the purpose of a meaningful comparison, all graphs are plotted in the same scale.

Successive hammer impact, as expected, not only causes a geometrical compaction due to further insertion of the prosthesis into the Sawbones block, but also increases the compressive stress in the parts. These two effects are shown in Fig. 12.

IV. DISCUSSION

Prevention of intraoperative fractures during prosthesis insertion while maximizing prosthesis-bone fixation and stability is a principal goal in THA. Further hammering ameliorates the fixation, but in the meantime may end up to a sudden fracture. In this study we proposed a new non-invasive vibrational analysis technique based on ESS as excitation and RFTE as response function to characterize, through the frequency shift analyses, the change in behavior of the artificial bone-prosthesis interface during the insertion. The results were compared to conventional FFT and its agreement with numerical finite element model was shown.

In the present approach, the metallic component (i.e., the prosthesis) was subject to vibrational testing while being in

direct dynamic contact with the artificial bone cavity during the insertion. At low frequencies, only bone undergoes deformation and the prosthesis behaves as a rigid boundary condition applied to the bone. But because of highly-damped nature of the system, excitation at low frequencies does not provide sufficient information on the vibrational characteristics of the system. Whereas, at high frequencies the surrounding bone behaves mainly as geometrical and natural boundary conditions applied to the prosthesis rather than a mass-spring. Therefore, excitation of prosthesis at a wide range of frequencies from few Hertz up to tens of thousands of Hertz increases the signal-to-noise ratio, and the reverberated vibrational wave contains enough energy to provide more information on the characteristics of the whole system.

Although the exponential sine signal is swept over the wide frequency range for thirty seconds (see Fig. 4(a)), the impulse response signal $h(t)$ is only few milliseconds because of natural damping (see Fig. 4(b)). As Fig. 5(b) illustrates, FFT of this impulse response signal has lower resolution compared to the RFTE of the extended signal. Moreover, bypassing the proposed technique and applying FFT directly to the measured signal $y(t)$ gives a noisy and inaccurate frequency spectrum compared to that obtained by our two-step procedure, as shown in Fig. 5(a). The main reason is that the sensor captures a lot of noise during the measurement, which are wideband from any other frequency. However, when looking at $h(t)$ at each instant of sweep, we are sending a known frequency, and deconvolution filter extracts the response at the same frequency and ignores other frequencies. Therefore, it is robust to noise. In a step further, where response function is enriched by prolonging $h(t)$ with the RFTE, this led to a better frequency resolution compared to frequency spectrum of $h(t)$.

It is also noticeable that upon successive hammering and further insertion of the prosthesis, frequency peaks in FFT(h) are becoming wide and weak due to increasing damping, as shown in blue in Fig. 6 at the insertion steps S_3 and S_{11} , and peak detection become difficult by a simple FFT, while they are still present in $H(f)$ at all insertion steps. Frequency peak enhancement by RFTE allows to trace adequately the variation of each natural frequency.

Frequency shifts as illustrated in Fig. 7 indicate three different types of evolution behavior: monotonically increasing (Group A), insensitive (Group B), and plateau-like (group C). As Fig. 10 shows, all prosthesis-Sawbones samples behave similarly and exhibit three distinct frequency evolution behavior with reasonably low standard deviations in order of only a few Hertz.

The frequency shift depends on the mode shape and not on the baseline frequency value. Some modes are more sensitive to the insertion depth, and some are not. The first two types do not individually provide useful information concerning the fixation evolution, whereas the frequency variation underlying in the third group reveals an important evolution trend. The Group C's frequencies increase by the hammer impactations until reaching a turning point, before the slope decreases until reaching a plateau, where further hammer impacts do not significantly change the frequencies. The absolute shift (with respect to the baseline state) remains almost constant, and no significant relative shift (with

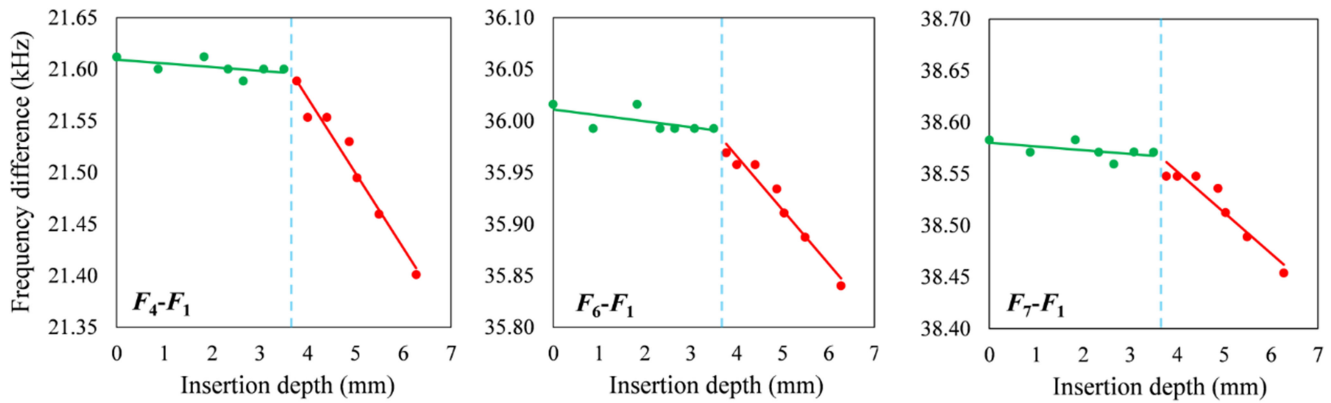


Fig. 9. Variations of inter-group frequency combinations (frequency difference) between Groups A and C with respect to insertion depth upon hammering.

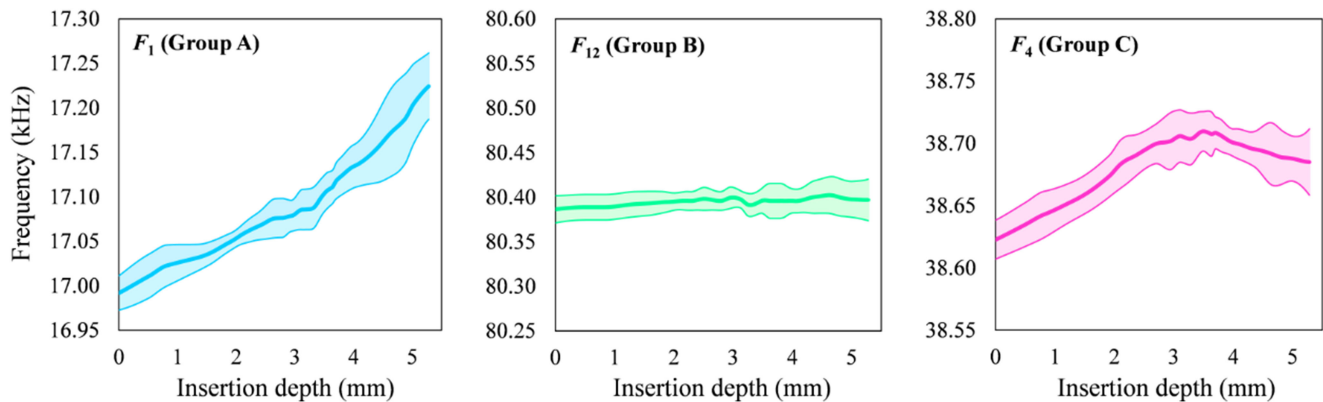


Fig. 10. Frequency evolution of three distinct categories (Groups A, B, and C) with respect to insertion depth upon hammering for all prosthesis-Sawbones samples (solid lines and shaded regions indicate the mean and standard deviation values over all prosthesis-Sawbones samples).

respect to the previous step) is observed. Similar phenomenon has also been observed in other studies where the absence of relative shift in the frequency spectrum is reported as an endpoint criterion for a sufficient fixation [7], [11]. These studies concluded also that further hammering not only does not change the frequencies, but also may result in fracture.

By analyzing higher frequencies within Group C, we noticed that some frequencies decreased after the plateau, as shown in Fig. 7(c). Moreover, the plateaus appear in different steps for different frequencies, although they all show similar trends.

The evolution trend observed in Group C can be explained by the fact that in prosthesis-Sawbones system the hammer impact undergoes two different mechanical phenomena with opposing effects on its vibrational characteristics. On one hand, after each hammering step, the prosthesis-Sawbones system gets smaller in size, and this geometrical compaction results in increase of natural frequencies. On the other hand, further hammering increases the compression between the parts which is known as a cause of decrease in natural frequencies [45]. In other words, by further insertion of prosthesis into the bone, the dynamic boundary condition around the prosthesis (i.e., the bone tissue) changes both geometrically by decrease of the size of whole system (due to increase of insertion depth) and naturally

by increase of interfacial contact stress. These two phenomena act in opposite ways.

It should be noted here that change of the interfacial contact area between the prosthesis and the bone has been addressed in previous studies [46] as another potential mechanism to describe the frequency shifts during the insertion. They suggested that increase of contact area during the insertion results in positive frequency shifts due to increase of structural integrity and apparent stiffness. However, these studies investigated pure effect of change of contact area without simulating the dynamic insertion of prosthesis into the bone cavity.

The two aforementioned concurrent mechanical phenomena have contradictory effects on the frequency evolution. Up to the turning point, the geometrical effect prevails over the compression effect, and the frequencies increase. By approaching towards the plateau, these phenomena somehow compromise, and there is almost no change in natural frequencies. Finally, this is the compression effect which plays the dominant role in the frequency evolution leading to frequency decrease. With this description, the two other evolution behavior observed in Groups A and B can also be justified. In Group A the mode shapes are less affected by the compression effect and the frequencies grow upon hammering monotonically, whereas the mode shapes

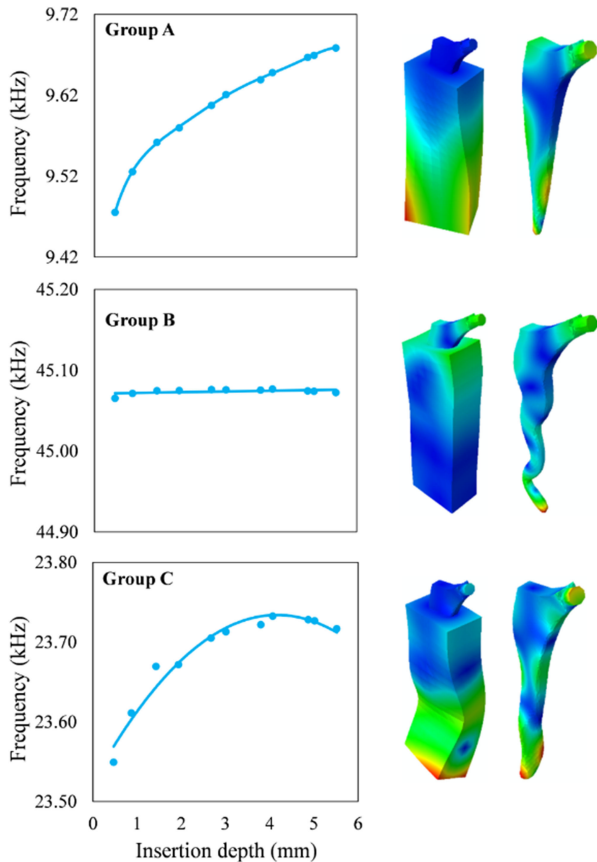


Fig. 11. Frequency evolution plots with respect to insertion depth and the associated mode shapes for the whole model and the prosthesis model for three indicative natural frequencies grouped in three distinct categories.

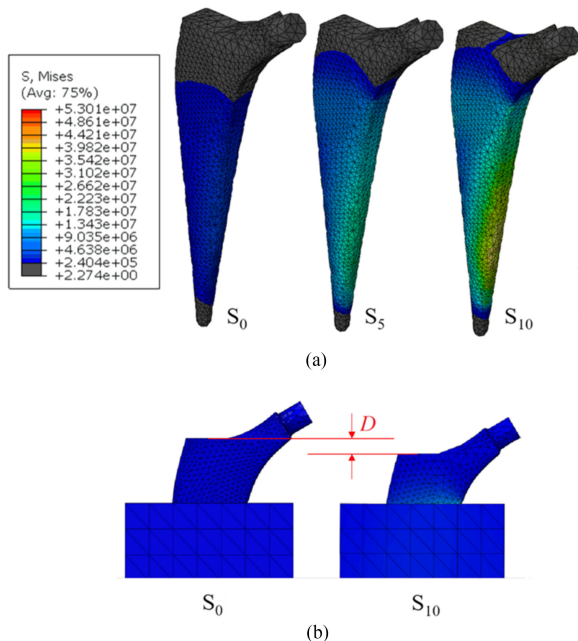


Fig. 12. Simulation results including (a) compressive von Mises stress distribution in the prosthesis for three sample steps (S_0 , S_5 , and S_{10}) and (b) the insertion depth from S_0 to S_{10} (calculated in the same way as measured in the experimental setup).

in Group B are either almost insensitive to both phenomena or affected in the same order.

Results of numerical simulation also confirm these observations. As illustrated in Fig. 11, tracing the variations of natural frequencies obtained by finite element modeling shows three distinct evolution behavior as previously observed in the experimental results. As shown in Fig. 12, the present finite element model captures both the opposing effects of compression and geometry compaction simultaneously, and therefore, it can well reflect the same evolution trends as observed experimentally. Nevertheless, numerical simulation is not expected to exactly predict the experimental results considering modeling simplifications in terms of geometrical details, material models, and contact mechanisms and properties.

With regards to these observations, a simple end-point criterion based on the individual frequency shift follow-ups may not be sufficient. Additional criterion based on combinatorial frequency analysis may provide useful information to warn the surgeon about further hammering. The mutual effects of aforementioned mechanical phenomena can be properly canceled out by intra- and inter-group frequency combinations. As shown in Fig. 8, the intra-group frequency combination in Group C depicts an apparent bilinear behavior with a distinct break point highlighted with a vertical dashed line. Fig. 9 also depicts a similar trend in the results of inter-group combination of frequencies of Groups A and C with the break points lying in the same place. This break point is obviously independent of intra- or inter-group frequency combinations, and therefore, can be a very good candidate for warning purposes.

In this study different advanced techniques were implemented in order to provide a robust detection of vibration frequencies. First, the ESS algorithm offered the advantage over other techniques such as the stepped-sine and the maximum length sequence (MLS), to have high signal-to-noise ratio [40] and low peak-to-RMS voltage ratio (known as crest factor) [47], [48], to last in few seconds with good frequency resolution [38], to be safe against the time variance [47], and to completely isolate the linear impulse response of the system from the nonlinear distortions [40]. As another advantage of the ESS, the deconvolution filter $d(t)$ defined in this technique depends only on the input signal, as shown in (5), and hence, is calculated only once. Consequently, the linear impulse response signal can be rapidly calculated after each hammering step according to (4) with considerably lower computational cost.

Nevertheless, unlike the linear sine sweep, the ESS sweeps faster over high frequencies than low frequencies, leading to a pink spectrum. Consequently, the non-uniform temporal distribution of excitation energy makes the signal spectrum not-flat [49]. This problem was resolved by Farina [39] upon the amplitude modulation of the time reversed signal. As an alternative, Meng *et al.* [49] implemented a pre-modulation to the input swept-sine signal to make the spectrum flat. Some other practical problems with the sweep signal synthesis in the time domain have also been resolved by its construction in the frequency domain [47]. A second implementation to enhance the frequency response was the application of recursive Fourier transform enhancement (RFTE) technique with the aim to mathematically

enrich the frequency spectrum by the impulse response signal prolongation in time domain. As depicted in Fig. 4(b), the response signal is too short in duration as a result of high structural damping. The more the prosthesis is inserted by hammer impactation, the shorter the response signal is collected due to increasing damping effect. On the other hand, the excitation power is limited to prevent invasion. Accordingly, the frequency spectrum obtained by the application of a simple FFT to the impulse response signal is not high amplitude enough to reflect distinguishable peaks.

As shown in Fig. 6, the frequency spectrum obtained by RFTE depicts high-amplitude and distinguishable peaks appropriate for the last analysis steps ahead to detect and label the dominant natural frequencies. As the frequency spectrum shows, the present vibrational measurement system, unlike the previous studies, is able to excite higher modes, which are more sensitive to fixation evolution.

To summarize the main achievements of the present study we should recall that the prosthesis-bone (or -Sawbones) system consists of a small massive metallic component (with higher natural frequencies and more complex vibrational modes) which is inserted into a long low-density porous material (with lower natural frequencies). Even the frequency sweep was between 0 and 100 kHz, at relatively low frequencies, only a very few vibrational modes of the system are excited. Although previous studies have shown that the low frequency analysis is still sensitive to evaluate the fixation quality, they confirmed that it is only capable of detection of prosthesis loosening at late stages (i.e., when the prosthesis is severely loose, and similarly, when the appropriate fixation is still not achieved during the insertion) [26]. Whereas sweeping over higher frequencies excites more complex mode shapes which are more sensitive to the fixation quality. It was thought in the early studies that the most sensitive band is above 2500 Hz [37]. More recent studies found out that higher natural frequencies are more sensitive to the prosthesis stability [36], [37]. For example, the most sensitive band for excitation was found above 4 kHz during the insertion of prosthesis in a THA [11], and between 12 and 15 kHz for the shoulder joint [18]. In the new vibrational technique presented in this paper, sweeping a sine signal from only few hundred Hertz up to tens of thousands of Hertz enabled us to excite a large number of high-power complex vibrational modes (that cannot be seen in low frequency bands). Hence, we could study the individual and combinatorial effects of different frequency evolution trends and establish a new criterion as an additional diagnostic tool which can warn the surgeon about the high-risk zone of hammering where further blows should be done cautiously to avoid the intraoperative fractures.

In spite of significant improvements presented in this paper for studying prosthesis fixation monitoring based on vibrational modal analysis, there are some limitations that need to be addressed in future works. Structural damping is the bottleneck of applying vibrational techniques to prosthesis fixation assessment. *In vivo* the presence of blood and bone marrow within the intramedullary canal introduces natural damping to the prosthesis-bone system which dissipates the vibration energy and decreases the peak values of natural frequencies, though it has no significant effect on the frequency values. Considering

that during rasping the bone marrow is almost evacuated, damping mainly arises from the remaining porous cancellous bone tissue. Therefore, to investigate the feasibility to pass this bottleneck, we performed our testing on spongy polyurethane foam. Moreover, to compensate the damping effect we introduced the RFTE algorithm to our vibrational measurement technique which mathematically enhances the frequency response function to contain sharp and distinct peaks.

As another limitation, it is noticeable that the spongy foam mimics only the cancellous bone structure, and the effect of composite cortical shell was omitted. Although the presence of outer cortical layer changes the frequency values, it does not affect the nature of frequency variations trend during hammering as we performed a similar test on a cylindrical sample made of the fourth generation of Sawbones composite samples.

Additionally, porosity and density of polyurethane foam is constant throughout the block, while the peri-prosthetic cancellous bone surrounding the implant is not of constant density or material property. To address this limitation, it is important to note that one of novelties in this technique is to investigate the evolution of vibrational characteristics of the metallic prosthesis (while being inserted) rather than the whole prosthesis-Sawbones system. In this way, the reverberated vibrational wave contains more energy, which enables us to determine the modal characteristics more accurately. In other words, in the presented approach the spongy foam surrounding the prosthesis behaves as a structural stiffness-damper in the whole system. With this in mind, varying density of cancellous bone mainly changes the equivalent damping with minor effect on the frequency shifts and overall evolution trends.

Numerical simulation presented in this paper modeled the prosthesis insertion in a linear elastic regime; however, it is clear that the insertion of prosthesis into a real bone causes interfacial plastic deformations (due to local breakage of cancellous structure) which may be a potential mechanism for describing the frequency variation trend observed in Group C.

Finally, we didn't find any informative mode (in terms of being distinguishable, traceable, and sharp) below 15 kHz, although the vibrational measurement and analysis was performed over a wide band from 800 Hz up to 96 kHz. As mentioned earlier this is due to the dominance of metallic massive implant compared to relatively small Sawbones block. In real bone with relatively larger dimension, we could expect a shift to lower band of the natural frequencies. Hence, additional *in vivo* tests on cadaveric specimens needs to be performed in order to further validate the present technique and improve the combinatorial analysis of frequency shifts during fixation of prosthesis in real bone.

V. CONCLUSION

Findings presented in this paper lead to the conclusion that, alongside the individual frequency shift follow-ups, the combinatorial analysis of frequency shifts provides objective information on the mechanical stability of Sawbone-prosthesis fixation. The proposed method allows to enhance frequency peak detection of prosthesis response function and trace these frequencies during the prosthesis insertion. This is very promising in providing the surgeon with an assistive diagnostic technique

during surgery by indicating when the bone-prosthesis fixation is acceptable, and beyond of which further hammering should be done cautiously to avoid bone fracture. Additional experiments in hip replacement with cadaveric specimens are necessary to further validate this method by comparison with the surgeon evaluation of prosthesis fixation and when hammering leads to fracture.

REFERENCES

- [1] D. J. Berry, *Fourth AJRR Annual Report on Hip and Knee Arthroplasty Data*, American Joint Replacement Registry, Rosemont, IL, 2017, pp. 1–71.
- [2] T. S. Brown *et al.*, “What’s new in total hip Arthroplasty,” *J. Bone Jt. Surgery-American Vol.*, vol. 96, no. 18, pp. 1576–1582, Sep. 2014.
- [3] K. A. Mann *et al.*, “Interface micromotion of uncemented femoral components from postmortem retrieved total hip replacements,” *J. Arthroplasty*, vol. 27, no. 2, pp. 238–245, Feb. 2012.
- [4] C. Zhang, C. H. Yan, and W. Zhang, “Cemented or cementless fixation for primary hip Arthroplasty—evidence from The International Joint Replacement Registries,” *Ann. Jt.*, vol. 2, pp. 57–57, Oct. 2017.
- [5] A. Crisman *et al.*, “Femoral component insertion monitoring using human cadaveric specimens,” in *Proc. 25th IMAC Conf. Struct. Dynamics*, 2007.
- [6] D. Y. R. Chong, U. N. Hansen, and A. A. Amis, “Analysis of bone–prosthesis interface micromotion for cementless tibial prosthesis fixation and the influence of loading conditions,” *J. Biomech.*, vol. 43, no. 6, pp. 1074–1080, Apr. 2010.
- [7] L. C. Pastrav *et al.*, “In vivo evaluation of a vibration analysis technique for the per-operative monitoring of the fixation of hip prostheses,” *J. Orthop. Surg. Res.*, vol. 4, no. 1, p. 10, 2009.
- [8] S. Szmukler-Moncler *et al.*, “Timing of loading and effect of micromotion on bone–dental implant interface: Review of experimental literature,” *J. Biomed. Mater. Res.*, vol. 43, no. 2, pp. 192–203, 1998.
- [9] M. Bahraminasab *et al.*, “Aseptic loosening of femoral components—A review of current and future trends in materials used,” *Mater. Des.*, vol. 42, pp. 459–470, Dec. 2012.
- [10] S. B. Goodman *et al.*, “Biocompatibility of total joint replacements: A review,” *J. Biomed. Mater. Res. Part A*, vol. 90A, no. 2, pp. 603–618, Aug. 2009.
- [11] L. C. Pastrav *et al.*, “Determination of total hip replacement stem insertion endpoint and stability assessment by vibration analysis,” in *Proc. ISMA 2006*, pp. 897–908.
- [12] C. C. Sidler-Maier and J. P. Waddell, “Incidence and predisposing factors of periprosthetic proximal femoral fractures: A literature review,” *Int. Orthop.*, vol. 39, no. 9, pp. 1673–1682, Sep. 2015.
- [13] R. M. D. Meek *et al.*, “Intraoperative fracture of the femur in revision total hip Arthroplasty with a diaphyseal fitting stem,” *J. Bone Jt. Surg.*, vol. 86-A, no. 3, pp. 480–485, 2004.
- [14] B. L. Penenberg *et al.*, “Digital Radiography in Total Hip Arthroplasty: technique and radiographic results,” *J. Bone Jt. Surg. Am.*, pp. 226–235, 2018.
- [15] S. Giardini *et al.*, “Monitoring femoral component insertion in cementless total hip Arthroplasty,” in *Proc. 23rd IMAC Conf. Struct. Dyn.*, 2005.
- [16] D. Abou-Trabi *et al.*, “Monitoring femoral component insertion during uncemented total hip Arthroplasty,” in *Proc. 24th IMAC Conf. Struct. Dyn.*, 2006.
- [17] M. Lannocca *et al.*, “Intra-operative evaluation of cementless hip implant stability: A prototype device based on vibration analysis,” *Med. Eng. Phys.*, vol. 29, no. 8, pp. 886–894, 2007.
- [18] L. Pastrav *et al.*, “Vibrational techniques to assess the stability of spherical press-fitted implants: Preliminary results,” in *Proc. Int. Conf. Noise Vib. Eng. Conf. Uncertainty Structural Dyn.*, 2010, pp. 1029–1044.
- [19] E. Varini *et al.*, “Assessment of implant stability of cementless hip prostheses through the frequency response function of the stem–bone system,” *Sensors Actuators, A Phys.*, vol. 163, no. 2, pp. 526–532, 2010.
- [20] F. Shao *et al.*, “Natural frequency analysis of osseointegration for transfemoral implant,” *Ann. Biomed. Eng.*, vol. 35, no. 5, pp. 817–824, 2007.
- [21] N. Cairns, *The Feasibility of Vibration Analysis as a Technique to Detect Osseointegration of Transfemoral Implants*. Brisbane, Australia: Queensland University of Technology, 2010.
- [22] C. Ruther *et al.*, “A novel sensor concept for optimization of loosening diagnostics in total hip replacement,” *J. Biomech. Eng.*, vol. 133, no. 10, 2011, Art. no. 104503.
- [23] C. Ruther *et al.*, “In vivo monitoring of implant osseointegration in a rabbit model using acoustic sound analysis,” *J. Orthop. Res.*, vol. 32, no. 4, pp. 606–612, 2014.
- [24] P. L. S. Li, N. B. Jones, and P. J. Gregg, “Vibration analysis in the detection of total hip prosthetic loosening,” *Med. Eng. Phys.*, vol. 18, no. 7, pp. 596–600, 1996.
- [25] A. P. Georgiou and J. L. Cunningham, “Accurate diagnosis of hip prosthesis loosening using a vibrational technique,” *Clin. Biomech.*, vol. 16, no. 4, pp. 315–323, 2001.
- [26] A. Rowlands, F. A. Duck, and J. L. Cunningham, “Bone vibration measurement using ultrasound: Application to detection of hip prosthesis loosening,” *Med. Eng. Phys.*, vol. 30, no. 3, pp. 278–284, 2008.
- [27] H. Ewald *et al.*, “A novel in vivo sensor for loosening diagnostics in total hip replacement,” in *Proc. IEEE Sensors*, 2011, pp. 89–92.
- [28] H. Ewald *et al.*, “Acoustic sensor system for loosening detection of hip implants,” in *Proc. Int. Conf. Sens. Technol.*, 2011, pp. 494–497.
- [29] J. S. Rieger *et al.*, “A vibrational technique for diagnosing loosened total hip endoprostheses: An experimental sawbone study,” *Med. Eng. Phys.*, vol. 35, no. 3, pp. 329–337, 2013.
- [30] A. A. Alshuhri *et al.*, “Development of a non-invasive diagnostic technique for acetabular component loosening in total hip replacements,” *Med. Eng. Phys.*, vol. 37, no. 8, pp. 739–745, 2015.
- [31] J. S. Rieger *et al.*, “Loosening detection of the femoral component of hip prostheses with extracorporeal shockwaves: A pilot study,” *Med. Eng. Phys.*, vol. 37, no. 2, pp. 157–164, 2015.
- [32] A. Arami *et al.*, “Knee implant loosening detection: A vibration analysis investigation,” *Ann. Biomed. Eng.*, vol. 46, no. 1, pp. 97–107, Jan. 2018.
- [33] S. Sauer and U. Marschner, “Medical wireless vibration measurement system for hip prosthesis loosening detection,” in *Proc. Sensordevices Third Int. Conf. Sens. Device Technol. Appl.*, 2012, pp. 9–13.
- [34] C. Ruther *et al.*, “Investigation of an acoustic-mechanical method to detect implant loosening,” *Med. Eng. Phys.*, vol. 35, no. 11, pp. 1669–1675, 2013.
- [35] R. Puers *et al.*, “Telemetry system for the detection of hip prostheses loosening by vibration analysis,” *Sensors Actuators, Phys.*, vol. 85, no. 1, pp. 42–47, 2000.
- [36] U. Marschner *et al.*, “Integration of a wireless lock-in measurement of hip prosthesis vibrations for loosening detection,” *Sensors Actuators, A Phys.*, vol. 156, no. 1, pp. 145–154, 2009.
- [37] G. Qi, W. Paul Mouchon, and T. E. Tan, “How much can a vibrational diagnostic tool reveal in total hip Arthroplasty loosening?” *Clin. Biomech.*, vol. 18, no. 5, pp. 444–458, Jun. 2003.
- [38] G. Gloth and M. Sinapius, “Detection of non-linearities in swept-sine measurements,” in *Proc. IMAC-21: A Conf. Expo. Structural Dyn.*, 2003.
- [39] A. Farina, “Simultaneous measurement of impulse response and distortion with a swept-sine technique,” in *Proc. AES 108th conv.*, 2000.
- [40] A. Farina, “Advancements in impulse response measurements by sine sweeps,” in *Proc. 122nd Conv. Audio Eng. Soc.*, 2007, p. 7121.
- [41] G. B. Stan, J. J. Embrechts, and D. Archambeau, “Comparison of different impulse response measurement techniques,” *J. Audio Eng. Soc.*, vol. 50, no. 4, pp. 249–262, 2002.
- [42] V. Liepins, “Extended Fourier analysis of signals,” Ph.D. dissertation, Univ. Latvia, Riga, Latvia, 1998.
- [43] [Online]. Available: https://www.sawbones.com/media/assets/product/documents/biomechanical_catalog.pdf
- [44] S. H. Pettersen, T. S. Wik, and B. Skallerud, “Subject specific finite element analysis of implant stability for a cementless femoral stem,” *Clin. Biomech.*, vol. 24, no. 6, pp. 480–487, Jul. 2009.
- [45] R. Bedri and M. O. Al-Nais, “Prestressed modal analysis using finite element package ANSYS,” *Lecture Notes Comput. Sci.*, vol. 3401, 2005, pp. 171–178.
- [46] L. C. Pastrav *et al.*, “A finite element analysis of the vibrational behaviour of the intra-operatively manufactured prosthesis–femur system,” *Med. Eng. Phys.*, vol. 31, no. 4, pp. 489–494, 2009.
- [47] S. Müller and P. Massarani, “Transfer-function measurement with sweeps,” *J. Audio Eng. Soc.*, vol. 49, no. 6, pp. 443–471, 2001.
- [48] I. H. Chan, “Swept sine chirps for measuring impulse response,” *Power (dBVrms)*, vol. 50, no. 40, p. 30, 2011.
- [49] Q. Meng *et al.*, “Impulse response measurement with sine sweeps and amplitude modulation schemes,” in *Proc. 2nd Int. Conf. Signal Process. Commun. Syst.*, 2008, pp. 1–5.